Materials Science & Engineering C 130 (2021) 112468

Contents lists available at ScienceDirect

Materials Science & Engineering C

journal homepage: www.elsevier.com/locate/msec

Poly(2-ethyl-2-oxazoline) functionalized reduced graphene oxide: Optimization of the reduction process using dopamine and application in cancer photothermal therapy

Rita Lima-Sousa [a], Cátia G. Alves [a], Bruna L. Melo [a], André F. Moreira [a], António G. Mendonça [a,b], Ilídio J. Correia [a,c,*], Duarte de Melo-Diogo [a,**]

[a] CICS-UBI – Centro de Investigação em Ciências da Saúde, Universidade da Beira Interior, 6200-506 Covilhã, Portugal
[b] Departamento de Química, Universidade da Beira Interior, 6201-001 Covilhã, Portugal
[c] CIEPQPF – Departamento de Engenharia Química, Universidade de Coimbra, 3030-790 Coimbra, Portugal

ARTICLE INFO

Keywords:
Cancer
Dopamine
Photothermal therapy
Poly(2-ethyl-2-oxazoline)
Reduced graphene oxide

ABSTRACT

The high near infrared (NIR) absorption displayed by reduced graphene oxide (rGO) nanostructures renders them a great potential for application in cancer photothermal therapy. However, the production of this material often relies on the use of hydrazine as a reductant, leading to poor biocompatibility and environmental-related issues. In addition, to improve rGO colloidal stability, this material has been functionalized with poly(ethylene glycol). However, recent studies have reported the immunogenicity of poly(ethylene glycol)-based coatings. In this work, the production of rGO, by using dopamine as the reducing agent, was optimized considering the size distribution and NIR absorption of the attained materials. The obtained results unveiled that the rGO produced by using a 1:5 graphene oxide:dopamine weight ratio and a reaction time of 4 h (termed as DOPA-rGO) displayed the highest NIR absorption while retaining its nanometric size distribution. Subsequently, the DOPA-rGO was functionalized with thiol-terminated poly(2-ethyl-2-oxazoline) (P-DOPA-rGO), revealing suitable physicochemical features, colloidal stability and cytocompatibility. When irradiated with NIR light, the P-DOPA-rGO could produce a temperature increase (ΔT) of 36 °C (75 μg/mL; 808 nm, 1.7 W/cm^2, 5 min). The photothermal therapy mediated by P-DOPA-rGO was capable of ablating breast cancer cells monolayers (viability < 3%) and could reduce heterotypic breast cancer spheroids' viability to just 30%. Overall, P-DOPA-rGO holds a great potential for application in breast cancer photothermal therapy.

1. Introduction

Nanomaterials with near infrared (NIR; 750–1000 nm) light absorption capacity have been the target of different studies for developing new anticancer photo-therapeutic approaches [1,2]. Due to their unique set of physicochemical properties, these nanomaterials can become accumulated at the tumor site by extravasating through the leaky tumor vasculature or through the dynamic vents occurring at the tumor site [3–5]. Then, the tumor zone is exposed to NIR light and the tumor-homed nanomaterials absorb its energy, releasing it as heat (photothermal therapy (PTT)) [6]. This photoinduced hyperthermia can induce damage to cancer cells, ultimately leading to their death by necrosis (generally attained when the local temperature surpasses 50 °C) [7].

Over the years, several NIR-responsive nanomaterials have been developed for application in cancer PTT, namely gold nanostructures [8–10], graphene derivatives [11,12], nanostructures encapsulating NIR-absorbing small molecules [13,14], among others. Particularly, the high NIR absorption of reduced graphene oxide (rGO) nanomaterials

Abbreviations: ANOVA, analysis of variance; CLSM, confocal laser scanning microscopy; DLS, dynamic light scattering; DMEM-F12, Dulbecco's modified Eagle's medium F-12; DOPA-rGO, rGO produced by using a 1:5 graphene oxide:dopamine weight ratio, for 4 h at 80 °C; FBS, fetal bovine serum; FTIR, Fourier-transform infrared spectroscopy; MCF-7, Michigan Cancer Foundation-7; NHDF, normal human dermal fibroblasts; NIR, near infrared; n.s., non-significant; P-DOPA-rGO, PEtOx-SH functionalized DOPA-rGO; PEG, poly(ethylene glycol); PEtOx-SH, thiol-terminated Poly(2-ethyl-2-oxazoline); PI, propidium iodide; PTT, photothermal therapy; RB, rhodamine B; rGO, reduced graphene oxide; SD, standard deviation.

* Correspondence to: I.J. Correia, CICS-UBI – Centro de Investigação em Ciências da Saúde, Universidade da Beira Interior, 6200-506 Covilhã, Portugal.
** Corresponding author.
E-mail addresses: icorreia@ubi.pt (I.J. Correia), demelodiogo@fcsaude.ubi.pt (D. de Melo-Diogo).

https://doi.org/10.1016/j.msec.2021.112468
Received 16 June 2021; Received in revised form 10 September 2021; Accepted 26 September 2021
Available online 2 October 2021

renders them a great potential for application in cancer PTT [6,15]. The chemical reduction of graphene oxide (a process that removes the oxygen-containing groups at its surface) is the most commonly applied route to obtain rGO [16]. For this purpose, hydrazine hydrate has been widely used as the reducing agent. However, the rGO attained using hydrazine hydrate lacks biocompatibility due to the toxicity of this reductant [17–19]. Recently, some studies have highlighted the potential of using dopamine as the reducing agent in the production of rGO [19–24]. During this process, dopamine also self-polymerizes, yielding rGO with a lattice covered by polydopamine [25]. Importantly, polydopamine is also a NIR absorber, and therefore the rGO attained by using dopamine can display a greatly improved photothermal capacity [25]. However, the experimental conditions to produce rGO by using dopamine have not yet been optimized considering the NIR absorption and the nanometric size distribution of the obtained materials.

Another concern related to the use of graphene-based nanomaterials in cancer PTT is associated to the weak water solubility and poor colloidal stability of these nanostructures [26,27]. These drawbacks have been surpassed by functionalizing the rGO surface with poly (ethylene glycol) (PEG) [26,28,29]. Unfortunately, it was unveiled that anti-PEG antibodies are created when PEGylated rGO is intravenously administered [30]. These anti-PEG antibodies mediate the rapid clearance of this nanomaterial in subsequent administrations (known as the accelerated blood clearance phenomenon) [31,32]. This immunogenic behavior has also been reported for other types of PEGylated nanomedicines, such as liposomes, polymeric nanoparticles, and even for FDA/EMA approved nanomedicines (*e.g.*, Doxil) [33–35]. Therefore, it is fundamental to investigate novel coatings to functionalize rGO nanomaterials.

In this work, and for the first time, the production of rGO by using dopamine as the reduction agent was optimized in order to obtain nanomaterials with a size distribution and NIR absorption suitable for application in cancer PTT. Additionally, the catechol-based surface of this rGO derivative was functionalized, for the first time, with thiol-terminated poly(2-ethyl-2-oxazoline) (PEtOx-SH) through a Michael addition reaction [36,37]. The selection of PEtOx was related to the growing use of this hydrophilic, biocompatible, and hemocompatible polymer as a PEG alternative [38,39]. Recently, our group also disclosed the potential of PEtOx-brushes for improving the colloidal stability of graphene-based nanostructures [11]. Furthermore, PEtOx-coated nanomaterials can exhibit a long blood circulation time due to their capacity to resist protein adsorption and uptake by macrophages, which is fundamental for their accumulation in the tumor zone [40–42].

The obtained data unveiled that the NIR absorption and size distribution of the rGO are affected by the dopamine content and the reaction time. In this regard, the rGO produced by using a 1:5 graphene oxide: dopamine weight ratio and a reaction time of 4 h (termed as DOPA-rGO) presented the highest NIR absorption while retaining its nanometric size distribution. Subsequently, the DOPA-rGO was functionalized with PEtOx-SH (P-DOPA-rGO), revealing suitable physicochemical properties, proper colloidal stability, and good cytocompatibility. When irradiated with NIR light for 5 min, the P-DOPA-rGO at 75 μg/mL (of DOPA-rGO equivalents) induced a temperature increase of 36 °C. The PTT mediated by P-DOPA-rGO was capable of ablating breast cancer cells monolayers (viability < 3%) and could reduce heterotypic breast cancer spheroids' viability to just 30%.

2. Materials and methods

2.1. Materials

Graphene oxide nanocolloids, PEtOx α-benzyl ω-thiol terminated (PEtOx-SH; average MW 10 000 Da), Dulbecco's modified Eagle's medium F-12 (DMEM-F12), penicillin/streptomycin, trypsin, rhodamine B (RB), paraformaldehyde and resazurin were bought from Sigma Aldrich (Sintra, Portugal). Dopamine hydrochloride was purchased from Acros Organics (New Jersey, USA). Sodium hydroxide was acquired from Labchem (Pennsylvania, USA). Tris-HCl was bought from Fisher Scientific (Oeiras, Portugal). Fetal bovine serum (FBS) was obtained from Biochrom AG (Berlin, Germany). Hoechst 33342® was bought from Invitrogen (Massachusetts, USA). Michigan Cancer Foundation-7 (MCF-7) cell line was acquired from ATCC (Middlesex, UK). Normal human dermal fibroblasts (NHDF) were obtained from Promo-Cell (Heidelberg, Germany). Calcein-AM was bought from Merck Milipore (Algés, Portugal) and propidium iodide (PI) from Alfa Aesar (Lancashire, UK). Cell culture plates and T-flasks were purchased from Thermo Fisher Scientific (Porto, Portugal). Agarose was acquired from GRiSP (Porto, Portugal). Cell imaging plates were acquired from Ibidi GmbH (Munich, Germany). Graphene oxide was firstly sonicated for 6 h before its use. Water used in all experiments was double deionized (0.22 μm filtered, 18.2 MΩ cm).

2.2. Methods

2.2.1. Optimization of the production of rGO by using dopamine

Firstly, the rGO production was optimized by using dopamine as the reducing agent and by adapting a protocol previously described elsewhere [23]. In brief, a solution of graphene oxide (500 μg/mL; 750 μL) was added to a round bottom flask. Subsequently, a dopamine solution (in order to obtain different graphene oxide:dopamine weight ratios (5:1, 1:1, 1:5 and 1:10)) and NaOH 10 mM were added. The solutions' final pH and volume were 8.5 and 1 mL, respectively. Then, the mixtures were left to react under stirring at 60 °C for 1, 2, 3, 4 or 5 h. Afterward, the samples were transferred to an ice-water bath in order to stop the reduction process. The size distribution of the obtained rGO nanomaterials was then characterized by dynamic light scattering (DLS) in a Zetasizer Nano ZS (Malvern Instruments, Worcestershire, UK) at a scattering angle of 173°. In turn, the materials' NIR absorption was evaluated by using an Evolution 201 spectrophotometer (Thermo Scientific Inc., Massachusetts, USA).

2.2.2. Production and characterization of PEtOx functionalized DOPA-rGO

The functionalization of DOPA-rGO with PEtOx-SH was performed by a Michael addition reaction [24,25]. Initially, the optimized rGO candidate was produced as described in Section 2.2.1 (by using a 1:5 graphene oxide:dopamine weight ratio and a reduction time of 4 h). Then, the obtained DOPA-rGO (200 μg/mL; 750 μL) was mixed with Tris-HCl (40 mM, 250 μL) and PEtOx-SH (1000 μg). This mixture was then sonicated for 2 h (Branson 5800, Branson Ultrasonics, CT, USA). Subsequently, the sample was dialyzed against water for 2 h (14 kDa molecular weight cut-off membrane) to remove NaOH, Tris-HCl and non-conjugated PEtOx-SH, yielding PEtOx-SH functionalized DOPA-rGO (P-DOPA-rGO). The DOPA-rGO used as control in all the subsequent experiments was also dialyzed.

The successful functionalization was confirmed by Fourier-transform infrared (FTIR) spectroscopy by using a Nicolet iS10 spectrometer (Thermo Scientific Inc., Massachusetts, USA). The size distribution of P-DOPA-rGO was analyzed by DLS and its ability to interact with NIR light was assessed by Visible-NIR absorption spectroscopy. The concentration of P-DOPA-rGO was determined using a standard curve of DOPA-rGO in water at 808 nm (PEtOx-SH does not display absorption at this wavelength). The zeta potential of P-DOPA-rGO and DOPA-rGO were also determined (Zetasizer Nano ZS). The size variation of P-DOPA-rGO during 48 h, when dispersed in cell culture medium (DMEM-F12 supplemented with 10% (v/v) of FBS), was also assessed.

The photothermal capacity of P-DOPA-rGO was investigated by following a protocol previously described by our group [43]. Concisely, P-DOPA-rGO at various concentrations was exposed to NIR light (808 nm, 1.7 W/cm^2) for a period of 5 min (n = 3). The temperature changes were recorded using a thermocouple thermometer. Water irradiated with NIR light was used as control.

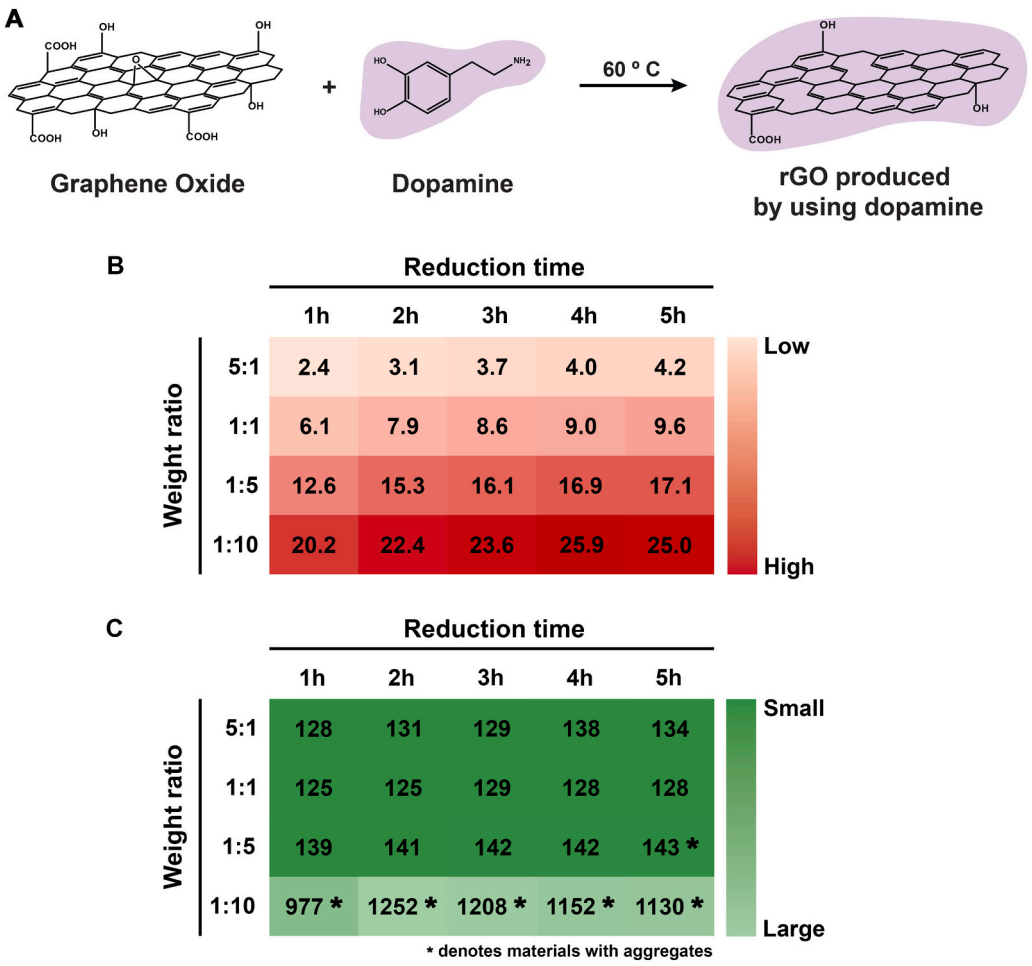

Fig. 1. Optimization of the protocol to produce rGO by using dopamine. Schematic representation of the protocol (A). Heat map graph of the materials' absorption at 808 nm normalized to the absorption of graphene oxide at this same wavelength (B). Heat map graph of the materials' size (z-average, in nm) (C). (*) denotes materials with aggregates.

2.2.3. Evaluation of the cytocompatibility of DOPA-rGO and P-DOPA-rGO

The cytocompatibility profile of the obtained nanomaterials was evaluated against breast cancer cells (MCF-7) and normal cells (NHDF), as previously described [12]. The cell lines were cultured in DMEM-F12 medium supplemented with 10% (v/v) FBS and 1% (v/v) of penicillin/streptomycin in a humified incubator at 37 °C, 5% CO_2. Then, the cells were harvested and seeded in 96-well plates at a density of 1×10^4 cells/well for 24 h. Subsequently, the cells were incubated with fresh medium containing DOPA-rGO or P-DOPA-rGO at different concentrations (of DOPA-rGO equivalents) for 24 or 48 h. Afterward, the medium was replaced by fresh medium containing resazurin (10% (v/v)) and following 4 h of incubation in the dark (37 °C, 5% CO_2), the cells' viability was assessed by analyzing the fluorescence of resorufin (λ_{ex} = 560 nm; λ_{em} = 590 nm) in a Spectramax Gemini EM spectrofluorometer (Molecular Devices LLC, California, USA) [44]. Cells only incubated with culture medium (without nanomaterials) were used as negative (K^-) control, whereas those treated with ethanol (70% (v/v)) represent the positive (K^+) control.

2.2.4. Evaluation of the cellular uptake of P-DOPA-rGO

Prior to the cellular uptake studies, P-DOPA-rGO (200 μg/mL, 1 mL) was fluorescently labelled with RB through a simple sonication process (30 min) [12]. Subsequently, the RB labelled P-DOPA-rGO was dialyzed against water for 90 min (1 kDa cut-off dialysis membrane) in order to remove the non-loaded RB.

The uptake of RB labelled P-DOPA-rGO by breast cancer cells was confirmed by confocal laser scanning microscopy (CLSM). In brief, MCF-7 cells were seeded in μ-slide 8-well imaging plates (Ibidi GmbH, Munich, Germany) at a density 1.5×10^4 cells/well, being allowed to grow for 48 h. Afterward, the cell culture medium was replaced by fresh culture medium containing RB labelled P-DOPA-rGO (50 μg/mL of DOPA-rGO equivalents). After 4 h, the medium was removed, and the cells were rinsed with a phosphate buffered saline solution and fixed with paraformaldehyde 4% (w/v) for 15 min (at room temperature). The cells' nucleus was labelled with Hoechst 33342® for 30 min (at room temperature) [45]. The fluorescence images were acquired ($\lambda_{ex}/\lambda_{em}$ = 405/410–499 nm (Hoechst 33342®) and $\lambda_{ex}/\lambda_{em}$ = 514/513–703 nm (RB)) in a Zeiss LSM 710 Confocal Microscope (Oberkochen, Germany). Non-treated cells were used as control.

2.2.5. Evaluation of the phototherapeutic effect of P-DOPA-rGO in 2D in vitro cancer models (monolayers of cancer cells)

The phototherapeutic effect mediated by P-DOPA-rGO against monolayers of breast cancer cells was evaluated by the resazurin method [46]. Briefly, MCF-7 cells were seeded in 96-well plates as described in Section 2.2.3. After 24 h of cells' seeding, the culture medium was replaced with fresh medium containing P-DOPA-rGO at different concentrations (50 and 75 μg/mL of DOPA-rGO equivalents). Four hours later, the cells were irradiated with NIR light (808 nm, 1.7 W/cm^2, 5 min). After 24 h of incubation with the nanomaterials, the cells' viability was determined through the resazurin assay as described in Section 2.2.3.

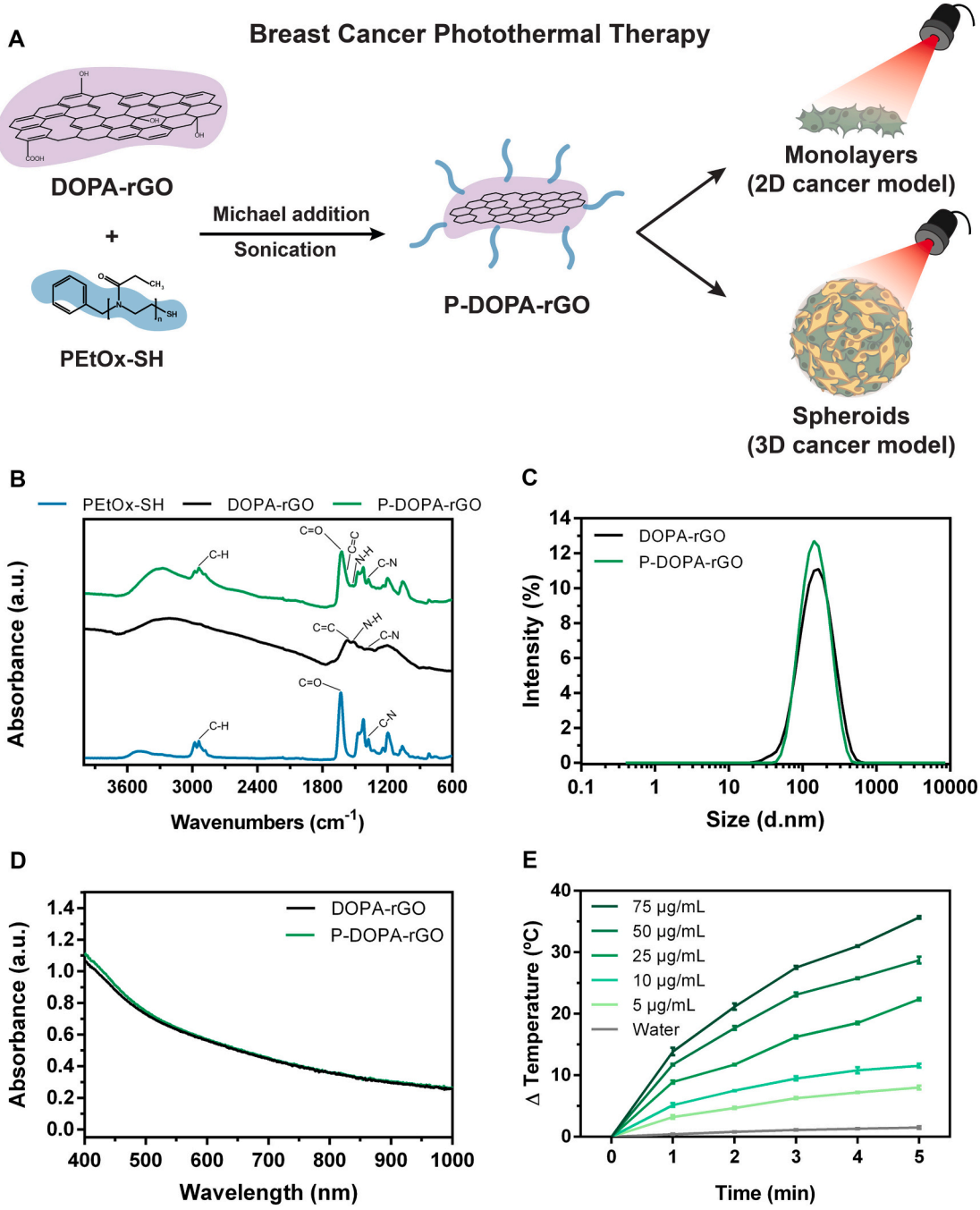

Fig. 2. Preparation and characterization of P-DOPA-rGO. Schematic representation of the functionalization of DOPA-rGO with PEtOx and its application in cancer PTT (A). FTIR spectra of PEtOx-SH, DOPA-rGO and P-DOPA-rGO (B). DLS size distribution of DOPA-rGO and P-DOPA-rGO (at 25 µg/mL of DOPA-rGO equivalents) (C). Visible-NIR absorption spectra of DOPA-rGO and P-DOPA-rGO (at 25 µg/mL of DOPA-rGO equivalents) (D). Temperature variation curves of P-DOPA-rGO at different concentrations (of DOPA-rGO equivalents) throughout 5 min of NIR light irradiation (1.7 W/cm^2, 808 nm) (n = 3) (E).

In order to visualize the phototherapeutic effect of P-DOPA-rGO, MCF-7 cells were seeded in µ-slide 8-well imaging plates as described in Section 2.2.4 and, 48 h later, the cells were incubated with fresh medium containing P-DOPA-rGO (at 50 and 75 µg/mL of DOPA-rGO equivalents) [43]. After 4 h of incubation, the cells were irradiated with NIR light (808 nm, 1.7 W/cm^2, 5 min). Subsequently, the cells were stained with Calcein-AM and PI (enables the visualization of live and dead cells, respectively) according to the manufacturer's protocol. The fluorescence images were acquired by CLSM, using a $\lambda_{ex}/\lambda_{em}$ of 488/493–556 (Calcein-AM) and 561/566–719 nm (PI) [43]. Cells solely incubated with culture medium were used as control for live cells.

2.2.6. Evaluation of the phototherapeutic effect of P-DOPA-rGO in 3D in vitro cancer models (spheroids)

The 3D heterotypic spheroids were produced as previously described by our group [47]. In brief, agarose (2% (w/v)) poured into a micromold (3D Petri Dish®, Microtissues Inc., Rhode Island, USA) was used to cast a hydrogel structure with spherical microwells. Then, MCF-7 cells and NHDF (1:1 cell ratio) were seeded into these structures at a density of 1 × 10^6 cells/structure. The spheroids were left to grow for 10 days in DMEM-F12 medium supplemented with 10% (v/v) FBS and 1% (v/v) of penicillin/streptomycin in a humified incubator at 37 °C, 5% CO_2. The culture medium was replaced every 2 days. The phototherapeutic effect

of P-DOPA-rGO was then determined using the resazurin method as previously described. Briefly, the spheroids were incubated with culture medium containing P-DOPA-rGO (at 50 and 75 μg/mL of DOPA-rGO equivalents) for 24 h. Then, the spheroids were irradiated with NIR light for 5 min (808 nm, 1.7 W/cm^2) and were further incubated for 48 h. After this period, the culture medium was replaced with fresh one containing resazurin (10% (v/v)). The cell viability was then determined as described in Section 2.2.3. Non-treated spheroids were used as negative control (K^-). Each experimental condition was tested in 30 spheroids.

In order to visualize the phototherapeutic effect of P-DOPA-rGO in spheroids, these were incubated with P-DOPA-rGO (at 75 μg/mL of DOPA-rGO equivalents). After 24 h, the spheroids were irradiated with NIR light (808 nm, 1.7 W/cm^2, 5 min). Lastly, the spheroids were stained with Calcein-AM/PI and the fluorescence images were acquired as described in Section 2.2.5.

2.2.7. Statistical analysis

For multiple groups comparison, the One-way analysis of variance (ANOVA) with the Student–Newman–Keuls test was utilized, and a p-value lower than 0.05 ($p < 0.05$) was considered statistically significant. The GraphPad Prism v6.0 (Trial version, GraphPad Software, CA, USA) was used for data analysis.

3. Results and discussion

3.1. Optimization of the production of rGO by using dopamine

Despite having a high photothermal capacity, the rGO produced by using hydrazine hydrate has a poor biocompatibility, which hinders its translation to the clinic [18,48]. To overcome this limitation, we optimized the production of rGO by using dopamine. In fact, dopamine has been previously proposed as an environmentally friendly reductant in the production of rGO [25,49]. During the reduction process, dopamine reduces the graphene oxide and self-polymerizes, yielding polydopamine-rGO hybrids. However, the experimental protocol for producing rGO by using dopamine has not yet been optimized considering the size distribution and NIR absorption of the attained materials. Therefore, we optimized the production of rGO by using dopamine by investigating the role of the i) graphene oxide:dopamine weight ratio, and ii) reduction time. For such, the content of graphene oxide was kept constant, and dopamine was added at the amounts required to achieve the graphene oxide:dopamine weight ratios of 5:1, 1:1, 1:5 and 1:10. Then, the reduction process was carried out at 60 °C for 1, 2, 3, 4 or 5 h (Fig. 1A).

In general, with the increase in the reaction's time and dopamine content fed, there was an increment on the NIR absorption of the attained materials (Figs. 1B and S1). In this regard, the highest NIR absorption was obtained for the rGO produced by using a 1:10 graphene oxide:dopamine weight ratio during 4 or 5 h of reaction, which displayed a 25.0–25.9-fold higher absorption at 808 nm than graphene oxide (Fig. 1B). Considering that 808 nm laser light will be used in the photothermal experiments, these candidates could potentially generate the highest photoinduced heat. However, all the rGO derivatives produced by using the 1:10 graphene oxide:dopamine weight ratio presented a size distribution in the micrometer range, hindering their application in cancer PTT (Figs. 1C and S2). The micrometer size distribution of these derivatives may be related to the aggregation of the materials during the reduction process.

Among the materials that retained their nanometric size distribution, the rGO obtained by using the 1:5 graphene oxide:dopamine weight ratio and 4 h of reaction displayed the greatest NIR absorption (16.9-fold higher absorption at 808 nm than graphene oxide). Therefore, the rGO produced using these parameters (DOPA-rGO) was selected for the subsequent assays.

For instance, Zhang *et al.* produced rGO by using a graphene oxide:dopamine weight ratio of 1:1, a temperature of 50 °C, and a reaction time of 24 h, that displayed approximately 12-fold higher absorption at 808 nm than graphene oxide [23]. Herein, the DOPA-rGO presented a 16.9-fold higher NIR absorption (at 808 nm than Graphene Oxide) and required a shorter reaction time (only 4 h). Therefore, the optimized DOPA-rGO production method presents a higher convenience.

3.2. Production and characterization of PEtOx functionalized DOPA-rGO

Next, DOPA-rGO was functionalized with PEtOx. For such, PEtOx-SH was conjugated to the catechol-based surface of DOPA-rGO through a Michael addition, yielding P-DOPA-rGO (Fig. 2A).

The successful functionalization of DOPA-rGO with PEtOx-SH was confirmed by FTIR (Fig. 2B). The FTIR spectrum of DOPA-rGO presented an intense peak at 1568 cm^{-1} belonging to the C═C stretch vibrations of rGO and polydopamine. As importantly, the DOPA-rGO did not display the C═O stretch peak of carboxylic acids (at 1730 cm^{-1}). This C═O stretch peak was present on the spectrum of graphene oxide (Fig. S3). Therefore, its absence on the FTIR spectrum of DOPA-rGO is also indicative of the successful reduction [50,51]. Furthermore, the peaks at 1373 cm^{-1} (C—N stretch) and 1516 cm^{-1} (N—H bend) in the DOPA-rGO spectrum also confirm the presence of polydopamine on this material [51]. On the other hand, the FTIR spectrum of PEtOx-SH presented peaks at 2976 cm^{-1} (C—H stretch) and 1628 cm^{-1} (C═O stretch from amides) [11,52]. Finally, the FTIR spectrum of P-DOPA-rGO presented the characteristic peaks of DOPA-rGO as well as those from PEtOx-SH, hence confirming the successful functionalization.

Furthermore, the DLS analysis revealed that the size distribution of the DOPA-rGO and P-DOPA-rGO were similar (Fig. 2C). Therefore, the PEtOx functionalization did not compromise the nanometric size distribution of P-DOPA-rGO, and thus the size of this nanomaterial is within the range considered as ideal for passive accumulation at the tumor site (100–200 nm) [53]. The zeta potential of DOPA-rGO (in water) was determined to be -22.2 ± 1.7 mV, whereas the one of P-DOPA-rGO was -26.5 ± 2.0 mV. These values are in line with those reported in the literature for rGO attained by using dopamine and for PEtOx-containing nanomaterials [23,54,55].

Additionally, the stability of P-DOPA-rGO over time in cell culture medium (DMEM-F12 supplemented with 10% (v/v) of FBS) was assessed to determine the suitability of the PEtOx functionalization. When dispersed in culture medium, the size of P-DOPA-rGO only increased by 3.1%, even after 48 h (Fig. S4), hence revealing an excellent colloidal stability.

Afterward, the NIR absorbance of the P-DOPA-rGO was analyzed (Fig. 2D). As it can be seen, the functionalization process did not affect the nanomaterials' NIR absorption, further confirming the suitability of the PEtOx functionalization (Fig. 2D).

Lastly, the photothermal capacity of P-DOPA-rGO was confirmed by irradiating this nanomaterial with NIR light for 5 min (808 nm, 1.7 W/cm^2) and analyzing the attained temperature variations. The P-DOPA-rGO generated a time- and concentration-dependent photoinduced heat (Fig. 2E). At the concentration of 75 μg/mL (of DOPA-rGO equivalents), the P-DOPA-rGO could induce a temperature increase of about 36 °C after 5 min of irradiation. Achieving this temperature increase is of utmost importance since it surpasses the threshold required to prompt the death of cancer cells by coagulative necrosis [7]. On the contrary, when water was irradiated with NIR radiation, it only suffered a temperature variation of 1.3 °C, which is in agreement with the low interaction of water with 808 nm light [6,12]. Such behavior suggests that P-DOPA-rGO may produce an on-demand photothermal effect with minimal off-target heating.

Jiang *et al.* recently produced rGO by using dopamine whose photothermal effect (at 50 μg/mL) led to a temperature increase of 23 °C (808 nm, 2 W/cm^2, 5 min) [56]. In another work, Yu and co-workers produced rGO by using dopamine that could induce a temperature increase of 19 °C (120 μg/mL, 880 nm, 1.5 W/cm^2, 5 min) [22]. Herein,

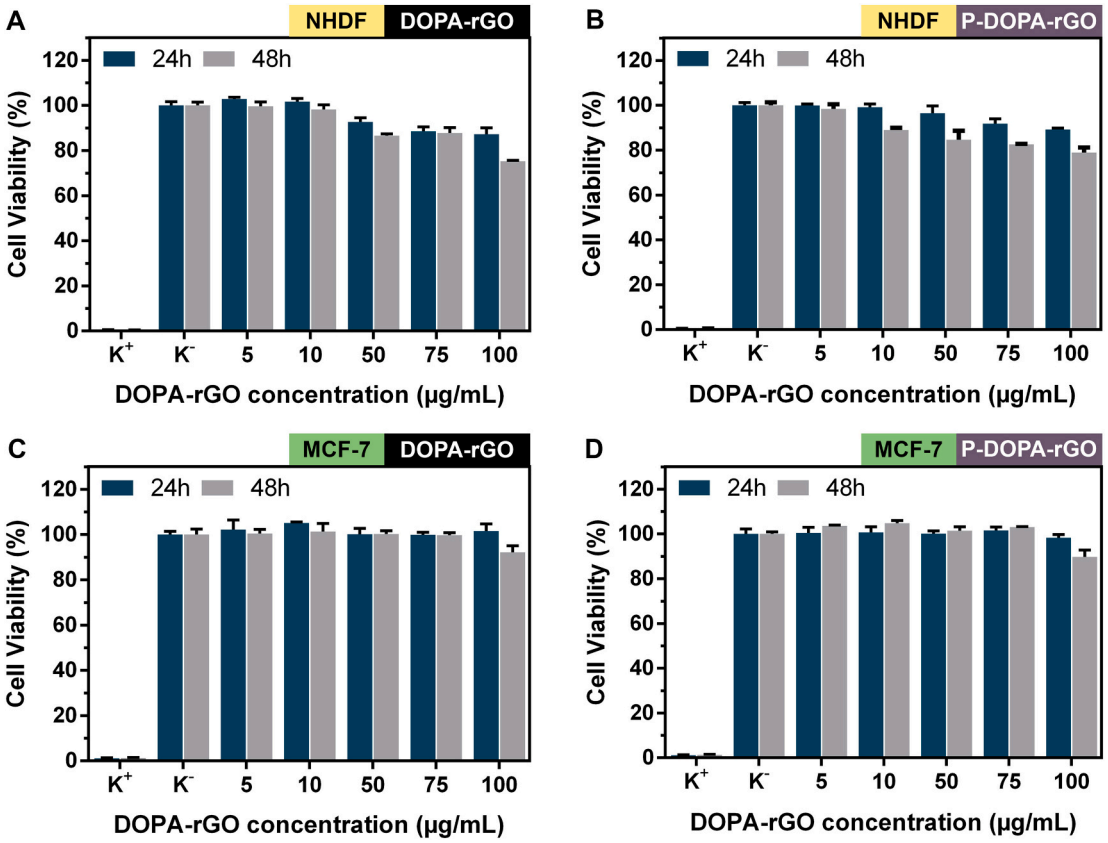

Fig. 3. Evaluation of the cytocompatibility profile of DOPA-rGO and P-DOPA-rGO at different concentrations. Cell viability of NHDF (A and B) and MCF-7 cells (C and D) exposed to DOPA-rGO and P-DOPA-rGO during 24 and 48 h of incubation. Data represents mean ± SD, n = 5. K^- and K^+ represent negative and positive controls, respectively.

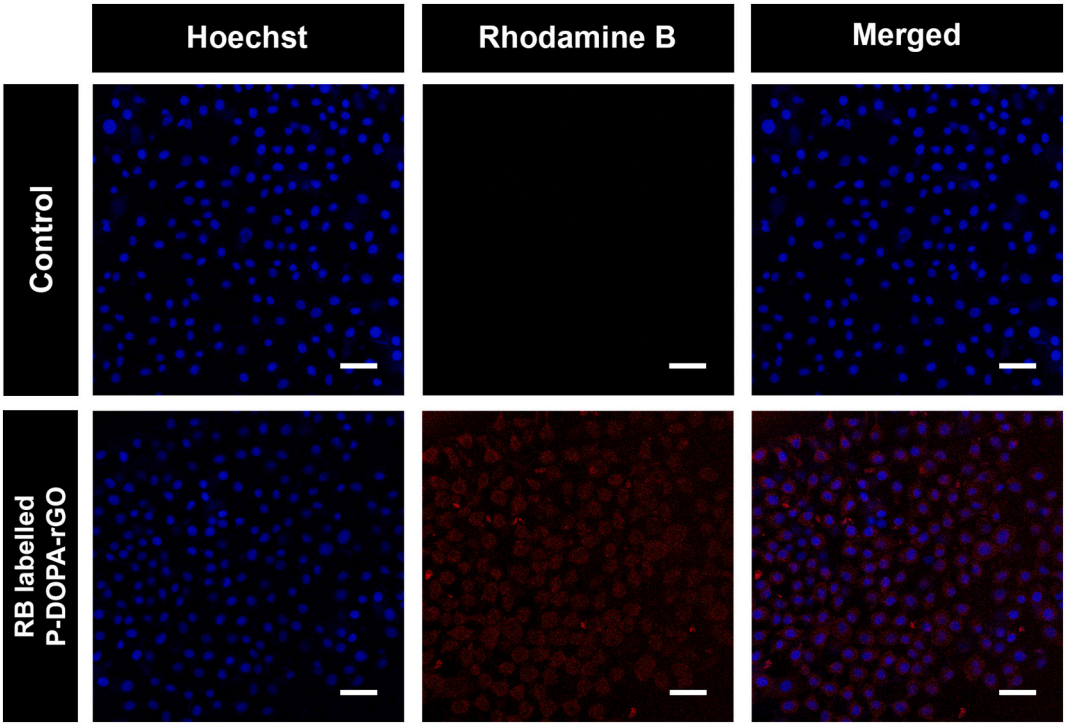

Fig. 4. Evaluation of the cellular uptake of RB labelled P-DOPA-rGO by MCF-7 cells through CLSM. Blue channel: Hoechst 33342® stained nucleus. Red channel: RB. Scale bars correspond to 50 μm. (For interpretation of the references to color in this figure legend, the reader is referred to the web version of this article.)

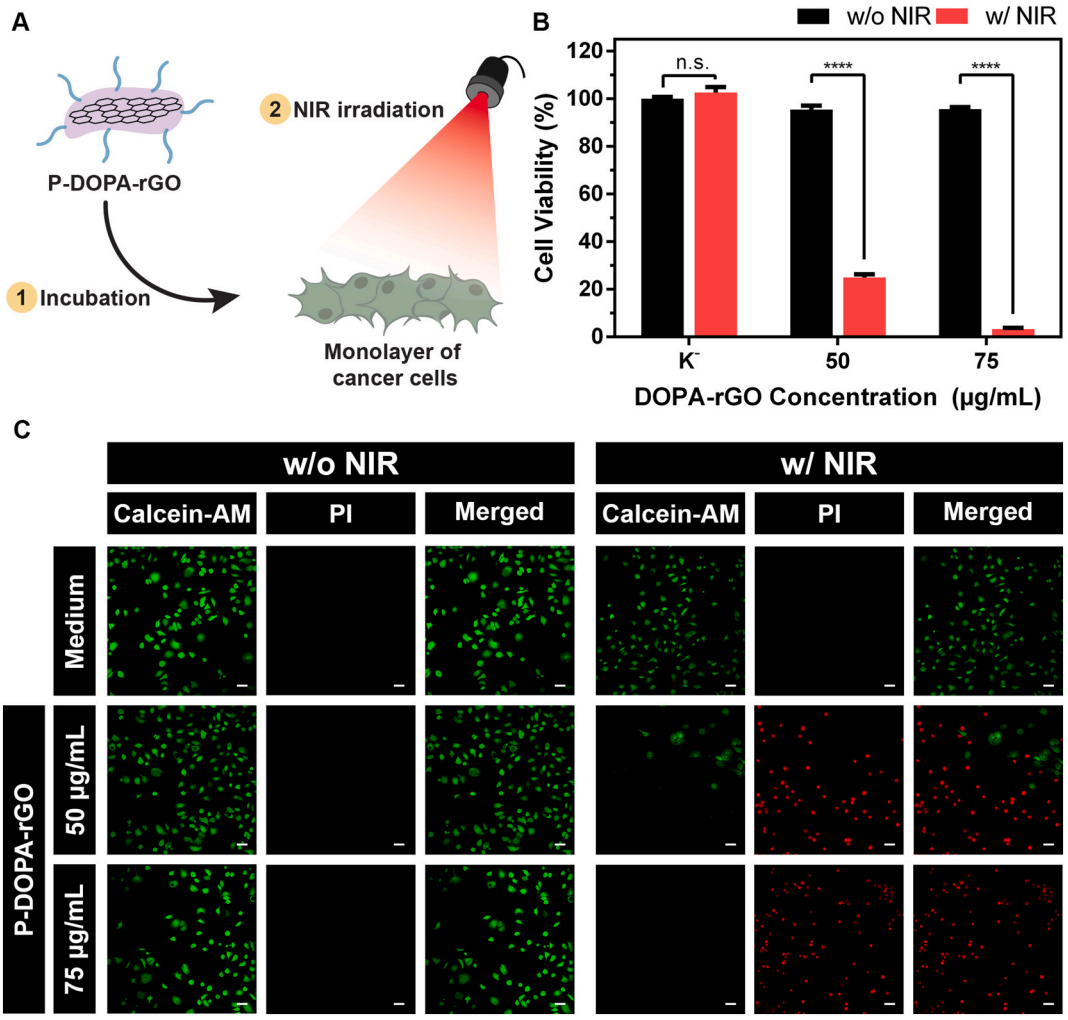

Fig. 5. Evaluation of the phototherapeutic capacity of P-DOPA-rGO in 2D *in vitro* cancer models. Schematic representation of the PTT mediated by P-DOPA-rGO (A). Effect of P-DOPA-rGO (at 50 and 75 μg/mL of DOPA-rGO equivalents) towards MCF-7 cells without NIR (w/o NIR) and with NIR (w/ NIR) laser irradiation (808 nm, 1.7 W/cm^2, 5 min) (B). K^- w/o NIR represents the negative control, whereas K^- w/ NIR represents cells solely exposed to NIR light. Data represents mean ± SD, n = 5 (****$p < 0.0001$), n.s. = non-significant. CLSM images of MCF-7 cells stained with Calcein-AM/PI after incubation with P-DOPA-rGO (at 50 and 75 μg/mL of DOPA-rGO equivalents) w/o NIR or w/ NIR laser irradiation (808 nm, 1.7 W/cm^2, 5 min) (C). Medium w/o NIR represents the control for live cells and medium w/ NIR represents cells only exposed to NIR light. Green channel: Calcein-AM; red channel: PI. Scale bars correspond to 50 μm. (For interpretation of the references to color in this figure legend, the reader is referred to the web version of this article.)

the P-DOPA-rGO at 50 μg/mL (of DOPA-rGO equivalents) could produce a photoinduced heat of 29 °C (808 nm, 1.7 W/cm^2, 5 min). This data suggests that the optimized DOPA-rGO synthesis enables the production of rGO derivatives with an improved photothermal capacity.

3.3. Evaluation of the cytocompatibility of DOPA-rGO and P-DOPA-rGO

Before determining the phototherapeutic potential of P-DOPA-rGO, the cytocompatibility profile of the different DOPA-rGO derivatives was investigated on MCF-7 cells (breast cancer cells) and NHDF (healthy human cells) (Fig. 3). For such, initially the effect of DOPA-rGO on cells' viability was investigated. Both cell lines exposed to DOPA-rGO remained highly viable (cell viability > 75%), even when incubated with a high nanomaterial's dose (100 μg/mL) and for 48 h – Fig. 3A and C. For instance, the rGO produced by using Vitamin C as reductant, at the concentration of 50 μg/mL, decreased the viability of NHDF to 51% after 48 h of incubation [12]. In other work, only 31% of the LNCaP cells exposed to rGO produced by using hydrazine hydrate (100 μg/mL) were viable after 24 h of incubation [48]. When compared to these alternative methods to attain rGO, the optimized DOPA-rGO presents a greatly improved cytocompatibility, which is crucial for biomedical- and cancer-related applications. This behavior is also in line with the good cytocompatibility profile of rGO nanomaterials produced by using dopamine reported elsewhere [20,21].

As expected, the P-DOPA-rGO also did not induce meaningful effects on NHDF (>79%) nor on MCF-7 cells (>90%), despite the high concentrations (up to 100 μg/mL of DOPA-rGO equivalents) and long incubation time (up to 48 h) tested (Fig. 3B and D). These results are also in line with the good cytocompatibility of PEtOx-based nanomaterials [57].

3.4. Evaluation of the cellular uptake of P-DOPA-rGO

Prior to evaluating the uptake of P-DOPA-rGO by MCF-7 cells, this nanomaterial was fluorescently labelled with RB to allow its visualization through CLSM. The successful labelling was confirmed by absorption spectroscopy (Fig. S5A), where the characteristic peak of RB can be visualized in the spectrum of RB labelled P-DOPA-rGO. As importantly, the RB labelling did not affect the size distribution of the attained nanomaterials (Fig. S5B).

Then, the uptake of RB labelled P-DOPA-rGO by MCF-7 cells was studied by CLSM (Fig. 4). RB fluorescent signals could be observed in the

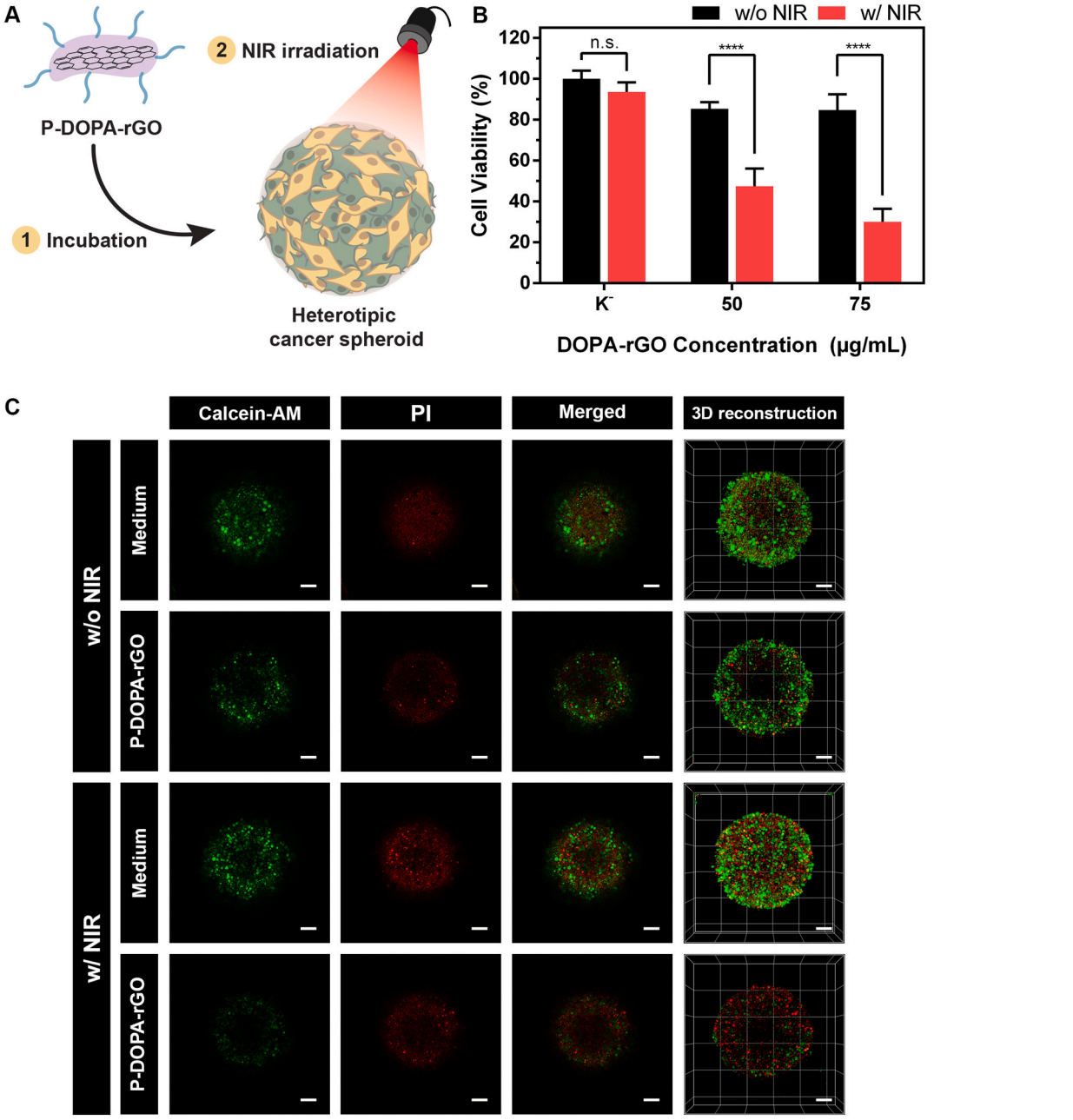

Fig. 6. Evaluation of the phototherapeutic capacity of P-DOPA-rGO in 3D *in vitro* cancer models (tumor spheroids). Schematic representation of the PTT mediated by P-DOPA-rGO towards spheroids (A). Effect of P-DOPA-rGO towards heterotypic spheroids without NIR (w/o NIR) and with NIR (w/ NIR) laser irradiation (808 nm, 1.7 W/cm^2, 5 min) (B). K^- w/o NIR represents the negative control, whereas K^- w/ NIR represents cells solely exposed to NIR light. Data represents mean ± SD, n = 30 (****$p < 0.0001$), n.s. = non-significant. CLSM images of spheroids stained with Calcein-AM/PI after incubation with P-DOPA-rGO (at 75 μg/mL of DOPA-rGO equivalents) w/o NIR or w/ NIR laser irradiation (808 nm, 1.7 W/cm^2, 5 min) (C). Medium w/o NIR and medium w/ NIR depict non-treated spheroids and spheroids only exposed to NIR light, respectively. Green channel: Calcein-AM; red channel: PI. Scale bars correspond to 100 μm. (For interpretation of the references to color in this figure legend, the reader is referred to the web version of this article.)

cytoplasm of MCF-7 cells incubated with RB labelled P-DOPA-rGO, indicating that this nanomaterial can successfully be internalized by breast cancer cells (Fig. 4). This behavior is in agreement with the good cellular uptake displayed by PEtOx-coated nanomaterials [55,58–60].

3.5. Evaluation of the phototherapeutic effect of P-DOPA-rGO in 2D in vitro cancer model (monolayers of cancer cells)

After confirming the *in vitro* safety of P-DOPA-rGO, the phototherapeutic capacity of this nanomaterial was evaluated on 2D *in vitro* cancer models. For such, monolayers of MCF-7 cells were incubated with P-DOPA-rGO (at the concentrations of 50 and 75 μg/mL of DOPA-rGO equivalents) and were irradiated with NIR light for 5 min (808 nm, 1.7 W/cm^2) (Fig. 5A).

As expected, non-irradiated P-DOPA-rGO did not affect meaningfully the cells' viability, being in line with the results reported in Section 3.3 (Fig. 3D). In turn, when MCF-7 cells were incubated with P-DOPA-rGO at 50 μg/mL (of DOPA-rGO equivalents) and irradiated with NIR light, their viability diminished to about 25% (Fig. 5B). The combined action of P-DOPA-rGO at 75 μg/mL (of DOPA-rGO equivalents) and NIR light could further decrease cells' viability to about 3%, leading to almost complete cancer cell ablation (Fig. 5B). It is also important to note that

breast cancer cells solely treated with NIR light did not suffer any alterations in their viability (Fig. 5B), which is supported by the weak/minimal interactions of NIR light with biological components [6]. These results were further confirmed through fluorescence images of Calcein-AM/PI stained MCF-7 cells exposed to P-DOPA-rGO in the presence and absence of NIR light (Fig. 5C).

Movahedi *et al.* developed folic acid-conjugated gold nanorods that could induce a decrease in KB cells' viability to about 35% after NIR laser irradiation (808 nm, 2 W/cm^2, 5 min; 15 μg/mL of nanoconjugates) [61]. Yu *et al.* verified that the PTT (808 nm, 2 W/cm^2, 5 min) mediated by rGO produced by using dopamine reduced MCF-7 cells' viability to 24% at a relatively high dose (120 μg/mL) [22]. Herein, the photothermal effect (808 nm, 1.7 W/cm^2, 5 min) mediated by P-DOPA-rGO reduced MCF-7 cells' viability to 3% at a moderate dose (75 μg/mL of DOPA-rGO equivalents). The P-DOPA-rGO improved phototherapeutic effect may be correlated with its good photothermal capacity and/or differences in the cellular internalization kinetics. In this way, P-DOPA-rGO is a promising nanomaterial for breast cancer PTT.

3.6. Evaluation of the phototherapeutic effect of P-DOPA-rGO in 3D in vitro cancer model (spheroids)

Then, the phototherapeutic capacity of P-DOPA-rGO was assessed in spheroids (Fig. 6A). Spheroids are 3D *in vitro* cancer models that can better mimic some features of the *in vivo* solid tumors (*e.g.*, 3D architecture, resistance to therapeutics' penetration (due to an increased interstitial fluid pressure)) [62,63]. Therefore, the use of spheroids has been growing due to their ability to better predict the efficacy of nanomedicines [63].

In accordance with the behavior observed in the 2D cancer models (Section 3.5.), the sole irradiation of the spheroids with NIR light or the administration of non-irradiated P-DOPA-rGO did not meaningfully affect the spheroids' viability (Fig. 6B). In turn, spheroids treated with P-DOPA-rGO (at 75 μg/mL of DOPA-rGO equivalents) plus NIR light had their viability decreased to just 30%. This lower efficacy of the phototherapeutic effect mediated by P-DOPA-rGO on spheroids when compared to that attained in the monolayers of cancer cells can be attributed to the higher spheroids' resistance to nanomaterials' penetration or to temperature mediated death [47,64].

Spheroids exposed to the aforementioned regiments were also stained with Calcein-AM/PI and imaged by CLSM. As it can be seen in Fig. 6C, the non-treated spheroids (medium w/o NIR) and the spheroids only irradiated with NIR light (medium w/ NIR light) mostly displayed an outer layer with Calcein-AM fluorescence and an inner layer with PI fluorescence (Fig. 6C). Such is in agreement with the layered organization of spheroids, which have an outer layer of highly proliferative cells and an inner core of necrotic cells [62]. In line with the cell viability results, spheroids incubated solely with P-DOPA-rGO demonstrated a Calcein-AM/PI staining quite similar to that of non-treated spheroids (Fig. 6C). On the other hand, spheroids treated with P-DOPA-rGO plus NIR light mainly displayed PI-stained with very few cells emitting Calcein-AM fluorescence (Fig. 6C), further corroborating the cell viability results.

In a recent work, Mó *et al.* unveiled that IR780 (photothermal agent; 9 μg/mL) and Doxorubicin (chemotherapeutic agent; 5.93 μg/mL) loaded polymeric nanoparticles can reduce spheroids' viability to 42% [47]. By combining this nanoformulation with NIR light (808 nm, 1.7 W/cm^2, 5 min), the spheroids' viability could be further diminished to 16% [47]. In this work, the non-irradiated P-DOPA-rGO had minimal effects on spheroids (viability $>$ 85%) while the combination of P-DOPA-rGO with NIR light was capable of decreasing spheroids' viability to 30% (75 μg/mL of DOPA-rGO equivalents; 808 nm, 1.7 W/cm^2, 5 min). In this way, the P-DOPA-rGO is a promising nanomaterial for on-demand phototherapeutic anti-cancer applications.

4. Conclusion

In this work, the production of rGO by using dopamine as the reduction agent was optimized, for the first time, in order to obtain nanomaterials with a size distribution and NIR absorption suitable for application in cancer PTT. Furthermore, the PEtOx-SH, a biocompatible PEG alternative, was used to functionalize, for the first time, the surface of the obtained DOPA-rGO through a Michael addition reaction. The obtained data unveiled that the NIR absorption and size distribution of the rGO are affected by the dopamine content and the reaction time. In this regard, the rGO produced by using a 1:5 graphene oxide:dopamine weight ratio and a reaction time of 4 h presented the highest NIR absorption while retaining its nanometric size distribution. Subsequently, the DOPA-rGO was functionalized with PEtOx-SH (P-DOPA-rGO), revealing suitable physicochemical properties, proper colloidal stability and good cytocompatibility. When irradiated with NIR light for 5 min, the P-DOPA-rGO at 75 μg/mL (of DOPA-rGO equivalents) induced a temperature increase of 36 °C. The PTT mediated by P-DOPA-rGO was capable of ablating breast cancer cells monolayers (viability $<$ 3%) and could reduce heterotypic breast cancer spheroids' viability to just 30%. Overall, P-DOPA-rGO holds a great potential for application in breast cancer PTT.

CRediT authorship contribution statement

Rita Lima-Sousa: Conceptualization, Investigation, Formal analysis, Writing - original draft. **Cátia G. Alves:** Investigation. **Bruna L. Melo:** Investigation. **André F. Moreira:** Investigation, Writing - review & editing. **António G. Mendonça:** Supervision, Writing - review & editing. **Ilídio J. Correia:** Project administration, Funding acquisition, Supervision, Writing - review & editing. **Duarte de Melo-Diogo:** Conceptualization, Investigation, Supervision, Writing - review & editing.

Declaration of competing interest

The authors declare that they have no known competing financial interests or personal relationships that could have appeared to influence the work reported in this paper.

Acknowledgements

This work was financed by the Foundation for Science and Technology (FCT), through funds from the State Budget, and by the European Regional Development Fund (ERDF), under the Portugal 2020 Program, through the Regional Operational Program of the Center (Centro2020), through the Project with the reference UIDB/00709/2020. The funding from CENTRO-01-0145-FEDER-028989 and POCI-01-0145-FEDER-031462 is also acknowledged. Duarte de Melo-Diogo acknowledges CENTRO-01-0145-FEDER-028989 for the funding given in the form of a research contract. Bruna L. Melo acknowledges POCI-01-0145-FEDER-031462 for the funding given in the form of a research fellowship. Rita Lima-Sousa and Cátia G. Alves acknowledge funding from individual PhD fellowships from FCT (SFRH/BD/144922/2019 and SFRH/BD/145386/2019, respectively).

Appendix A. Supplementary data

Supplementary data to this article can be found online at https://doi.org/10.1016/j.msec.2021.112468.

References

[1] A.C.V. Doughty, A.R. Hoover, E. Layton, C.K. Murray, E.W. Howard, W.R. Chen, Nanomaterial applications in photothermal therapy for cancer, Materials 12 (5) (2019) 779.

[2] X. Li, J.F. Lovell, J. Yoon, X. Chen, Clinical development and potential of photothermal and photodynamic therapies for cancer, Nat. Rev. Clin. Oncol. 17 (11) (2020) 657–674.
[3] S.K. Golombek, J.-N. May, B. Theek, L. Appold, N. Drude, F. Kiessling, T. Lammers, Tumor targeting via EPR: strategies to enhance patient responses, Adv. Drug Deliv. Rev. 130 (2018) 17–38.
[4] Y. Matsumoto, J.W. Nichols, K. Toh, T. Nomoto, H. Cabral, Y. Miura, R.J. Christie, N. Yamada, T. Ogura, M.R. Kano, Y. Matsumura, N. Nishiyama, T. Yamasoba, Y. H. Bae, K. Kataoka, Vascular bursts enhance permeability of tumour blood vessels and improve nanoparticle delivery, Nat. Nanotechnol. 11 (6) (2016) 533–538.
[5] J. Park, Y. Choi, H. Chang, W. Um, J.H. Ryu, I.C. Kwon, Alliance with EPR effect: combined strategies to improve the EPR effect in the tumor microenvironment, Theranostics 9 (26) (2019) 8073–8090.
[6] D. de Melo-Diogo, R. Lima-Sousa, C.G. Alves, I.J. Correia, Graphene family nanomaterials for application in cancer combination photothermal therapy, Biomater. Sci. 7 (9) (2019) 3534–3551.
[7] K.F. Chu, D.E. Dupuy, Thermal ablation of tumours: biological mechanisms and advances in therapy, Nat. Rev. Cancer 14 (3) (2014) 199–208.
[8] M. Mirrahimi, J. Beik, M. Mirrahimi, Z. Alamzadeh, S. Teymouri, V.P. Mahabadi, N. Eslahi, F. Ebrahimi Tazehmahalleh, H. Ghaznavi, A. Shakeri-Zadeh, C. Moustakis, Triple combination of heat, drug and radiation using alginate hydrogel co-loaded with gold nanoparticles and cisplatin for locally synergistic cancer therapy, Int. J. Biol. Macromol. 158 (2020) 617–626.
[9] Z. Alamzadeh, J. Beik, M. Mirrahimi, A. Shakeri-Zadeh, F. Ebrahimi, A. Komeili, B. Ghalandari, H. Ghaznavi, S.K. Kamrava, C. Moustakis, Gold nanoparticles promote a multimodal synergistic cancer therapy strategy by co-delivery of thermo-chemo-radio therapy, Eur. J. Pharma. Sci. 145 (2020) 105235.
[10] J. Beik, M. Asadi, S. Khoei, S. Laurent, Z. Abed, M. Mirrahimi, A. Farashahi, R. Hashemian, H. Ghaznavi, A. Shakeri-Zadeh, Simulation-guided photothermal therapy using MRI-traceable iron oxide-gold nanoparticle, J. Photochem. Photobiol. B Biol. 199 (2019) 111599.
[11] D. de Melo-Diogo, E.C. Costa, C.G. Alves, R. Lima-Sousa, P. Ferreira, R.O. Louro, I. J. Correia, POxylated graphene oxide nanomaterials for combination chemo-phototherapy of breast cancer cells, Eur. J. Pharm. Biopharm. 131 (2018) 162–169.
[12] R. Lima-Sousa, D. de Melo-Diogo, C.G. Alves, E.C. Costa, P. Ferreira, R.O. Louro, I. J. Correia, Hyaluronic acid functionalized green reduced graphene oxide for targeted cancer photothermal therapy, Carbohydr. Polym. 200 (2018) 93–99.
[13] C.G. Alves, D. de Melo-Diogo, R. Lima-Sousa, I.J. Correia, IR780 loaded sulfobetaine methacrylate-functionalized albumin nanoparticles aimed for enhanced breast cancer phototherapy, Int. J. Pharm. 582 (2020) 119346.
[14] S. Li, Z. Sun, G. Deng, X. Meng, W. Li, D. Ni, J. Zhang, P. Gong, L. Cai, Dual-modal imaging-guided highly efficient photothermal therapy using heptamethine cyanine-conjugated hyaluronic acid micelles, Biomater. Sci. 5 (6) (2017) 1122–1129.
[15] F. Alemi, R. Zarezadeh, A.R. Sadigh, H. Hamishehkar, M. Rahimi, M. Majidinia, Z. Asemi, A. Ebrahimi-Kalan, B. Yousefi, N. Rashtchizadeh, Graphene oxide and reduced graphene oxide: efficient cargo platforms for cancer theranostics, J. Drug Deliv. Sci. Technol. 60 (2020) 101974.
[16] V. Agarwal, P.B. Zetterlund, Strategies for reduction of graphene oxide – a comprehensive review, Chem. Eng. J. 405 (2021) 127018.
[17] T.A. Tabish, M.Z.I. Pranjol, H. Hayat, A.A.M. Rahat, T.M. Abdullah, J.L. Whatmore, S. Zhang, In vitro toxic effects of reduced graphene oxide nanosheets on lung cancer cells, Nanotechnology 28 (50) (2017) 504001.
[18] S.M. Hussain, J.M. Frazier, Cellular toxicity of hydrazine in primary rat hepatocytes, Toxicol. Sci. 69 (2) (2002) 424–432.
[19] S. Thakur, N. Karak, Alternative methods and nature-based reagents for the reduction of graphene oxide: a review, Carbon 94 (2015) 224–242.
[20] D. Hu, J. Zhang, G. Gao, Z. Sheng, H. Cui, L. Cai, Indocyanine green-loaded polydopamine-reduced graphene oxide nanocomposites with amplifying photoacoustic and photothermal effects for cancer theranostics, Theranostics 6 (7) (2016) 1043.
[21] L. Shao, R. Zhang, J. Lu, C. Zhao, X. Deng, Y. Wu, Mesoporous silica coated polydopamine functionalized reduced graphene oxide for synergistic targeted chemo-photothermal therapy, ACS Appl. Mater. Interfaces 9 (2) (2017) 1226–1236.
[22] J. Yu, Y.H. Lin, L. Yang, C.C. Huang, L. Chen, W.C. Wang, G.W. Chen, J. Yan, S. Sawettanun, C.H. Lin, Improved anticancer photothermal therapy using the bystander effect enhanced by antiarrhythmic peptide conjugated dopamine-modified reduced graphene oxide nanocomposite, Adv. Healthcare Mater. 6 (2) (2017) 1600804.
[23] X. Zhang, X. Nan, W. Shi, Y. Sun, H. Su, Y. He, X. Liu, Z. Zhang, D. Ge, Polydopamine-functionalized nanographene oxide: a versatile nanocarrier for chemotherapy and photothermal therapy, Nanotechnology 28 (29) (2017) 295102.
[24] Z. Zhu, M. Su, Polydopamine nanoparticles for combined chemo-and photothermal cancer therapy, Nanomaterials 7 (7) (2017) 160.
[25] L.Q. Xu, W.J. Yang, K.-G. Neoh, E.-T. Kang, G.D. Fu, Dopamine-induced reduction and functionalization of graphene oxide nanosheets, Macromolecules 43 (20) (2010) 8336–8339.
[26] Z. Liu, J.T. Robinson, X. Sun, H. Dai, PEGylated nanographene oxide for delivery of water-insoluble cancer drugs, J. Am. Chem. Soc. 130 (33) (2008) 10876–10877.
[27] Y. Li, L. Feng, X. Shi, X. Wang, Y. Yang, K. Yang, T. Liu, G. Yang, Z. Liu, Surface coating-dependent cytotoxicity and degradation of graphene derivatives: towards the design of non-toxic, degradable nano-graphene, Small 10 (8) (2014) 1544–1554.
[28] Z. Xu, S. Zhu, M. Wang, Y. Li, P. Shi, X. Huang, Delivery of paclitaxel using PEGylated graphene oxide as a nanocarrier, ACS Appl. Mater. Interfaces 7 (2) (2015) 1355–1363.
[29] R. Costa-Almeida, D. Bogas, J.R. Fernandes, L. Timochenco, F.A. Silva, J. Meneses, I.C. Gonçalves, F.D. Magalhães, A.M. Pinto, Near-infrared radiation-based mild photohyperthermia therapy of non-melanoma skin cancer with PEGylated reduced nanographene oxide, Polymers 12 (8) (2020) 1840.
[30] N. Luo, J.K. Weber, S. Wang, B. Luan, H. Yue, X. Xi, J. Du, Z. Yang, W. Wei, R. Zhou, PEGylated graphene oxide elicits strong immunological responses despite surface passivation, Nat. Commun. 8 (1) (2017) 1–10.
[31] P. Zhang, F. Sun, S. Liu, S. Jiang, Anti-PEG antibodies in the clinic: current issues and beyond PEGylation, J. Control. Release 244 (2016) 184–193.
[32] K. Shiraishi, M. Yokoyama, Toxicity and immunogenicity concerns related to PEGylated-micelle carrier systems: a review, Sci. Technol. Adv. Mater. 20 (1) (2019) 324–336.
[33] M. Ichihara, T. Shimizu, A. Imoto, Y. Hashiguchi, Y. Uehara, T. Ishida, H. Kiwada, Anti-PEG IgM response against PEGylated liposomes in mice and rats, Pharmaceutics 3 (1) (2011) 1–11.
[34] W. Lu, J. Wan, Z. She, X. Jiang, Brain delivery property and accelerated blood clearance of cationic albumin conjugated pegylated nanoparticle, J. Control. Release 118 (1) (2007) 38–53.
[35] T. Suzuki, M. Ichihara, K. Hyodo, E. Yamamoto, T. Ishida, H. Kiwada, H. Ishihara, H. Kikuchi, Accelerated blood clearance of PEGylated liposomes containing doxorubicin upon repeated administration to dogs, Int. J. Pharm. 436 (1–2) (2012) 636–643.
[36] N. Shahkaramipour, C.K. Lai, S.R. Venna, H. Sun, C. Cheng, H. Lin, Membrane surface modification using thiol-containing zwitterionic polymers via bioadhesive polydopamine, Ind. Eng. Chem. Res. 57 (6) (2018) 2336–2345.
[37] C.-Y. Liu, C.-J. Huang, Functionalization of polydopamine via the aza-michael reaction for antimicrobial interfaces, Langmuir 32 (19) (2016) 5019–5028.
[38] M. Bauer, C. Lautenschlaeger, K. Kempe, L. Tauhardt, U.S. Schubert, D. Fischer, Poly (2-ethyl-2-oxazoline) as alternative for the stealth polymer poly (ethylene glycol): comparison of in vitro cytotoxicity and hemocompatibility, Macromol. Biosci. 12 (7) (2012) 986–998.
[39] K. Knop, R. Hoogenboom, D. Fischer, Schubert U.S., Poly (ethylene glycol) in drug delivery: pros and cons as well as potential alternatives, Angew. Chem., Int. Ed. 49 (36) (2010) 6288–6308.
[40] A. Mero, G. Pasut, L. Dalla Via, M.W. Fijten, U.S. Schubert, R. Hoogenboom, F. M. Veronese, Synthesis and characterization of poly(2-ethyl 2-oxazoline)-conjugates with proteins and drugs: suitable alternatives to PEG-conjugates? J. Control. Release 125 (2) (2008) 87–95.
[41] N. Gao, C. Xing, H. Wang, L. Feng, X. Zeng, L. Mei, Z. Peng, pH-responsive dual drug-loaded nanocarriers based on poly (2-ethyl-2-oxazoline) modified black phosphorus nanosheets for cancer chemo/photothermal therapy, Front. Pharmacol. 10 (2019) 270.
[42] P. Wilson, P.C. Ke, T.P. Davis, K. Kempe, Poly(2-oxazoline)-based micro- and nanoparticles: a review, Eur. Polym. J. 88 (2017) 486–515.
[43] B.L. Melo, R. Lima-Sousa, C.G. Alves, P. Ferreira, A.F. Moreira, I.J. Correia, D. de Melo-Diogo, Sulfobetaine methacrylate-albumin-coated graphene oxide incorporating IR780 for enhanced breast cancer phototherapy, Nanomedicine 16 (6) (2021) 453–464.
[44] I.J. Sabino, R. Lima-Sousa, C.G. Alves, B.L. Melo, A.F. Moreira, I.J. Correia, D. de Melo-Diogo, Injectable in situ forming hydrogels incorporating dual-nanoparticles for chemo-photothermal therapy of breast cancer cells, Int. J. Pharm. 600 (2021) 120510.
[45] T.A. Jacinto, C.F. Rodrigues, A.F. Moreira, S.P. Miguel, E.C. Costa, P. Ferreira, I. J. Correia, Hyaluronic acid and vitamin E polyethylene glycol succinate functionalized gold-core silica shell nanorods for cancer targeted photothermal therapy, Colloids Surf. B 188 (2020) 110778.
[46] M.M. Leitão, C.G. Alves, D. de Melo-Diogo, R. Lima-Sousa, A.F. Moreira, I. J. Correia, Sulfobetaine methacrylate-functionalized graphene oxide-IR780 nanohybrids aimed at improving breast cancer phototherapy, RSC Adv. 10 (63) (2020) 38621–38630.
[47] I. Mó, C.G. Alves, D. de Melo-Diogo, R. Lima-Sousa, I.J. Correia, Assessing the combinatorial chemo-photothermal therapy mediated by sulfobetaine methacrylate-functionalized nanoparticles in 2D and 3D in vitro cancer models, Biotechnol. J. 15 (12) (2020) 2000219.
[48] O. Akhavan, E. Ghaderi, S. Aghayee, Y. Fereydooni, A. Talebi, The use of a glucose-reduced graphene oxide suspension for photothermal cancer therapy, J. Mater. Chem. 22 (27) (2012) 13773–13781.
[49] B.S. Dash, G. Jose, Y.-J. Lu, J.-P. Chen, Functionalized reduced graphene oxide as a versatile tool for cancer therapy, Int. J. Mol. Sci. 22 (6) (2021) 2989.
[50] N. Huang, S. Zhang, L. Yang, M. Liu, H. Li, Y. Zhang, S. Yao, Multifunctional electrochemical platforms based on the Michael addition/Schiff base reaction of polydopamine modified reduced graphene oxide: construction and application, ACS Appl. Mater. Interfaces 7 (32) (2015) 17935–17946.
[51] S. Zhang, D. Zhang, Z. Li, Y. Yang, M. Sun, Z. Kong, Y. Wang, H. Bai, W. Dong, Polydopamine functional reduced graphene oxide for enhanced mechanical and electrical properties of waterborne polyurethane nanocomposites, J. Coat. Technol. Res. 15 (6) (2018) 1333–1341.
[52] J. Yang, L. Li, C. Ma, X. Ye, Degradable polyurethane with poly (2-ethyl-2-oxazoline) brushes for protein resistance, RSC Adv. 6 (74) (2016) 69930–69938.
[53] E. Blanco, H. Shen, M. Ferrari, Principles of nanoparticle design for overcoming biological barriers to drug delivery, Nat. Biotechnol. 33 (9) (2015) 941–951.

[54] C.-H. Lin, Y.-C. Chen, P.-I. Huang, Preparation of multifunctional dopamine-coated zerovalent iron/reduced graphene oxide for targeted phototheragnosis in breast cancer, Nanomaterials 10 (10) (2020) 1957.
[55] H. Zhang, X. Liu, T. Xu, K. Xu, B. Du, Y. Li, Biodegradable reduction and pH dual-sensitive polymer micelles based on poly (2-ethyl-2-oxazoline) for efficient delivery of curcumin, RSC Adv. 10 (43) (2020) 25435–25445.
[56] W. Jiang, F. Mo, Y. Lin, X. Wang, L. Xu, F. Fu, Tumor targeting dual stimuli responsive controllable release nanoplatform based on DNA-conjugated reduced graphene oxide for chemo-photothermal synergetic cancer therapy, J. Mater. Chem. B 6 (26) (2018) 4360–4367.
[57] J. Tian, H. Zhou, R. Jiang, J. Chen, L. Mao, M. Liu, F. Deng, L. Liu, X. Zhang, Y. Wei, Preparation and biological imaging of fluorescent hydroxyapatite nanoparticles with poly(2-ethyl-2-oxazoline) through surface-initiated cationic ring-opening polymerization, Mater. Sci. Eng. C 108 (2020) 110424.
[58] A.F. Moreira, C.F. Rodrigues, C.A. Reis, E.C. Costa, P. Ferreira, I.J. Correia, Development of poly-2-ethyl-2-oxazoline coated gold-core silica shell nanorods for cancer chemo-photothermal therapy, Nanomedicine 13 (20) (2018) 2611–2627.
[59] O. Sedlacek, B.D. Monnery, J. Mattova, J. Kucka, J. Panek, O. Janouskova, A. Hocherl, B. Verbraeken, M. Vergaelen, M. Zadinova, R. Hoogenboom, M. Hruby, Poly(2-ethyl-2-oxazoline) conjugates with doxorubicin for cancer therapy: in vitro and in vivo evaluation and direct comparison to poly[N-(2-hydroxypropyl) methacrylamide] analogues, Biomaterials 146 (2017) 1–12.
[60] M. Xu, C. Yao, W. Zhang, S. Gao, H. Zou, J. Gao, Anti-cancer activity based on the high docetaxel loaded poly(2-oxazoline)s micelles, Int. J. Nanomedicine 16 (2021) 2735–2749.
[61] M.M. Movahedi, A. Mehdizadeh, F. Koosha, N. Eslahi, V.P. Mahabadi, H. Ghaznavi, A. Shakeri-Zadeh, Investigating the photo-thermo-radiosensitization effects of folate-conjugated gold nanorods on KB nasopharyngeal carcinoma cells, Photodiagn. Photodyn. Ther. 24 (2018) 324–331.
[62] E.C. Costa, A.F. Moreira, D. de Melo-Diogo, V.M. Gaspar, M.P. Carvalho, I. J. Correia, 3D tumor spheroids: an overview on the tools and techniques used for their analysis, Biotechnol. Adv. 34 (8) (2016) 1427–1441.
[63] A.S. Nunes, A.S. Barros, E.C. Costa, A.F. Moreira, I.J. Correia, 3D tumor spheroids as in vitro models to mimic in vivo human solid tumors resistance to therapeutic drugs, Biotechnol. Bioeng. 116 (1) (2019) 206–226.
[64] I. Mó, I.J. Sabino, D. de Melo-Diogo, R. Lima-Sousa, C.G. Alves, I.J. Correia, The importance of spheroids in analyzing nanomedicine efficacy, Nanomedicine 15 (15) (2020) 1513–1525.